

# Structure of superheavy nuclei

**Michael Bender**

Univ. Bordeaux, CENBG, UMR5797, F-33175 Gradignan, France, and  
CNRS/IN2P3, CENBG, UMR5797, F-33175 Gradignan, France

E-mail: [bender@cenbg.in2p3.fr](mailto:bender@cenbg.in2p3.fr)

**Paul-Henri Heenen**

Physique Nucléaire Théorique, Université Libre de Bruxelles, C.P. 229, B-1050 Bruxelles, Belgium

**Abstract.** Properties of transactinide nuclei needed for the interpretation of spectroscopic data and for the extrapolation to the expected "island of stability" of superheavy nuclei are reviewed from a theorist's point of view in the framework of self-consistent mean-field models.

## 1. Introduction

Superheavy elements (SHE) are usually defined as the chemical elements whose atomic nuclei have a vanishing fission barrier in the liquid drop model. In this schematic picture, for nuclei with  $Z \gtrsim 106$  the strong Coulomb repulsion pushes the nucleus to large deformation and overcomes the surface tension that tries to keep the nucleus at small deformation. That such systems can exist and have been indeed observed is due to quantal shell effects: according to Strutinski's theorem, a less than average density of single-particle levels around the Fermi energy gives additional binding, whereas a larger than average value reduces the binding. As a consequence, the variation of the single-particle spectrum with deformation creates local pockets and barriers in the deformation energy surface. Being on a scale of about 10 MeV, the amplitude of these variations is small compared to the total binding energy of almost 2 GeV, but it is large enough to stabilise many heavy nuclei against spontaneous fission.  $\alpha$ -decay,  $\beta$ -decay or electron capture often become their dominating decay modes instead. SHE are also often called *transactinides*.

Over the last four decades, the limits of the chart of nuclei have been pushed far into the realm of superheavy elements up to  $Z = 118$  [1, 2, 3, 4, 5, 6, 7]. One motivation for the experimental efforts in this field of nuclear research is the long-standing prediction of an island of very long-living spherical SHE, which originally was expected to be centred at  $Z \approx 114$  and  $N \approx 184$  [8, 9, 10, 11, 12]. Even when the expectations about their lifetimes had to be cut down from years or even longer to minutes, perhaps just seconds, finding such nuclei would still provide a unique laboratory to study the nuclear many-body system under extreme conditions.

Because of the quickly dropping fusion cross sections [1, 2, 3, 4, 5, 13], the number of events for the production of elements with  $Z \gtrsim 104$  is very low, ranging from just a few to a few dozen. Consequently, the information available for these nuclei is limited to their existence (where even the attribution of a neutron number is sometimes a matter of debate), their dominating decay channel (usually fission or  $\alpha$  decay) and corresponding lifetime, and in case of  $\alpha$ -decay also the

$Q_\alpha$  value. For some odd- $A$  nuclei the branching of  $\alpha$ -decay into different levels in the daughter nucleus is observed already at this low level of statistics. Not only the properties of the atomic nuclei are studied for these heavy elements, but also some of their basic chemical properties [14].

Detailed spectroscopic information about their nuclear structure is available only for nuclei up to the lower border of the region of transactinides, for  $Z$  values up to about 104 [15, 16, 17, 18, 19]. These can be produced in much larger quantities and have longer lifetimes than most of the (known) heavier nuclides, such that they can be studied with a wide range of experimental setups. Electromagnetic transitions within and between rotational bands up to quite high spin are obtained from in-beam spectroscopy. Not only ground-state bands are studied, but there is also an increasing body of data for bands build on  $K$  isomers [20, 21]. Complementary information is obtained from decay spectroscopy of stopped ions. It provides detailed information about  $\gamma$  transitions from  $K$  isomers,  $\alpha$ -decay transition energies, lifetimes, branching ratios for transitions to different levels in the daughter nuclei, and also information about electromagnetic transitions in the daughter nuclei. As in many cases the daughter nuclei are  $\alpha$  emitters themselves, one experiment usually provides data for several nuclei [22, 23]. Finally, ion traps can be used to measure ground-state properties. The latter technique has been added only very recently to the arsenal of heavy-element research. The first pioneering experiments delivered the masses of a few nuclides around  $^{254}\text{No}$  [24]. Up to now, the quantum numbers of energy levels have been directly determined only for some heavy nuclei up to  $Z \simeq 100$ , cf. [15, 18, 19] and references therein. For heavier nuclei, the attribution of quantum numbers has to be based on arguments about selection rules for transitions, which sometimes leads to conflicting spin assignments or even level schemes when the experiments are performed with different set-ups and analysed by different groups. Again, the production cross section limits spectroscopic studies to the most favourable cases of projectile and target combinations.

The experimental efforts are closely accompanied by theoretical studies. Mean-field models are the tools of choice for the description of the structure of transactinides. They come in two different forms, *macroscopic-microscopic models* on the one hand, and *self-consistent mean-field models* on the other hand. Macroscopic-microscopic models [8, 25, 26, 27, 28, 29] combine the "macroscopic" energy  $E_{\text{mac}}$  of a droplet of nuclear matter and a Strutinski shell correction  $E_{\text{mic}}$  that is calculated from the single-particle spectrum obtained from some parametrised single-particle potential. Both are calculated for a common shape parametrised by a set of coefficients  $\{\alpha_i\}$ ,  $E_{\text{tot}}[\{\alpha_i\}] = E_{\text{mac}}[\{\alpha_i\}] + E_{\text{mic}}[\{\alpha_i\}]$ . There are many variants [30] that differ in the higher-order and deformation-dependent terms of the liquid drop and the form of the single-particle potential. A calculation consists in scanning the multi-dimensional energy surface for a given family of nuclear shapes for minima. By contrast, the entirely microscopic self-consistent mean-field models [31], used in the form of HF+BCS or HFB, have as solution a set of single-particle wave functions  $\{\psi_i\}$  that minimises the binding energy  $E_{\text{tot}}[\{\psi_i\}]$  from a given effective interaction and thereby provides local minima in the energy surface. Still, the surface can be mapped with the help of Lagrange multipliers. There are many variants that differ in the form of the effective interaction. The most widely used ones are the non-relativistic contact Skyrme [32, 33, 34, 35, 36, 37, 38, 39, 40, 41, 42, 43] and finite-range Gogny interactions [44, 45, 46, 47, 48] as well as relativistic mean-fields (RMF) [35, 36, 37, 49, 50, 51, 52, 53, 54, 55, 56] that are also called covariant density functional theory. The macroscopic-microscopic method can be obtained as an approximation to self-consistent models [57]. In what follows, the concept of a shell correction will be used for the intuitive interpretation of the results from self-consistent mean-field calculations, even when it is not an ingredient of the model.

Both methods have their specific advantages and disadvantages that are often complementary. The major technical advantages of the microscopic-macroscopic approaches are their numerical simplicity, that the parametrisations of the "macroscopic" and "microscopic" parts can be optimised separately, and that continuous multi-dimensional energy surfaces for fission or fusion

can be easily constructed. The price to be paid is that this approach cannot describe the feedback of the single-particle wave functions onto the mean field, and that the convergence of the results in terms of higher-order shape parameters is difficult to control [28]. There is a multitude of parametrisations of the nuclear surface to be found in the literature [58], some of which are better adapted to compact shapes, whereas others are better suited for very elongated shapes and the transition to situations with two centres. The advantages of the self-consistent models are that due to their variational nature they automatically optimise all shape degrees of freedom not fixed by global symmetries and that they incorporate the feedback of the single-particle wave functions on the mean field. The latter is not only important for the description of polarisation effects driven by the Coulomb field, but also for the description of alignment effects in rotational bands and of the rearrangement of the nucleus when constructing  $K$  isomers. Extensions of self-consistent models can be used to calculate correlations such as quantum fluctuations in shape degrees of freedom [59, 60]. In addition, their time-dependent variants can be used for the study of certain aspects of the production of heavy elements [61]. Their main disadvantage is that the currently used effective interactions are not yet flexible enough to provide the same level of accuracy for the description of heavy nuclei as the macroscopic-microscopic models, and that the construction of continuous multi-dimensional deformation energy surfaces needed for fission studies with the help of constraints and Lagrange multipliers is technically challenging.

The following sections will discuss three aspects of the structure of superheavy nuclei that are important for the extrapolation to the island of stability based on the available spectroscopic information in the  $Z \approx 100$  region. We will focus on self-consistent mean-field models. Section 2 presents predictions for single-particle spectra of spherical SHE, whereas Section 3 addresses deformed shell structure. Section 4 will explore the role of correlations beyond the mean field on the structure of SHE. Finally, Section 5 summarises the discussion.

## 2. Spherical shell structure

Shell structure of transactinide and superheavy nuclei is usually discussed in terms of the spectrum of eigenvalues  $\epsilon_\mu$  of the single-particle Hamiltonian  $\hat{h}$

$$\hat{h} \psi_\mu(\mathbf{r}) = \frac{\delta E_{\text{tot}}}{\delta \psi_\mu^\dagger(\mathbf{r})} = \epsilon_\mu \psi_\mu(\mathbf{r}) \quad (1)$$

in even-even nuclei. They reflect the mean field in the nucleus and provide a zeroth-order approximation to separation energies. It has to be stressed that there is no unique way of defining a single-particle energy, and that most definitions are model-dependent. The shell structure of light nuclei is often discussed in terms of single-particle energies that are associated with the centroids of the strength function for nucleon pick-up and stripping reactions, cf. Ref. [62, 63] and references therein. These cannot be expected to be equivalent to those from Eq. (1).

Even after more than forty years of experimental and theoretical efforts, the question where are the next closed spherical proton and neutron shells beyond  $^{208}\text{Pb}$  is still open. There is no evidence that there are singly-magic spherical ones among the superheavy nuclei observed in experiment so far, and there is no consensus among theorists with regard to the location of the island of stability. Concerning predictions for shell structure, the main challenges for theory are:

- (i) The models have to be extrapolated far beyond the region where their parametrisations were adjusted. The reliability of the extrapolation of nuclear structure models has rarely been quantified so far. For mean-field models, first steps into this direction were taken just recently for the extrapolation to the neutron drip line at large proton-to-neutron ratio [64].
- (ii) The average density of single-particle levels around the Fermi energy increases with particle number. As a consequence, the spacing of single-particle levels is much smaller than the

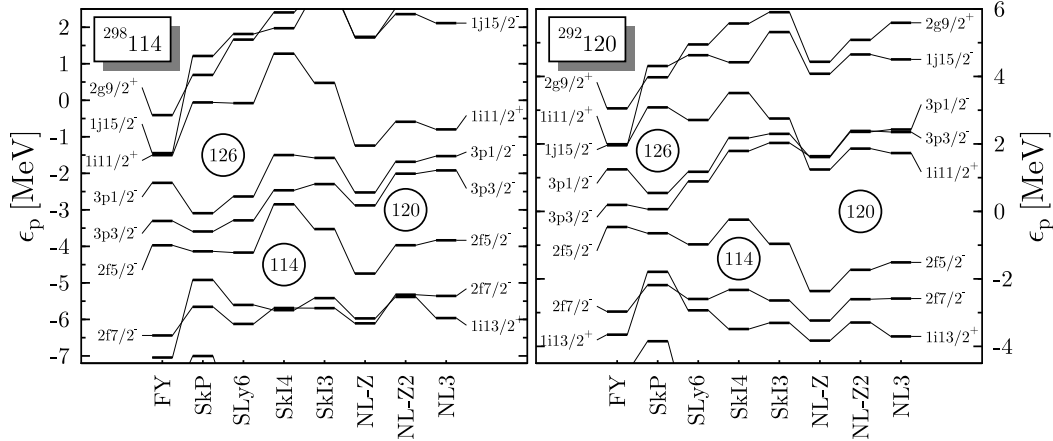


**Figure 1.** Proton single-particle spectra for  $^{298}_{184}114$  (left panel) and  $^{292}_{172}120$  (right panel) obtained with the folded-Yukawa single-particle potential used in macroscopic-microscopic models (FY), the Skyrme interactions SkP, SLy6, SkI4 and SkI3, and the NL-Z, NL-Z2 and NL3 parametrisations of the RMF. Data taken from Ref. [37].

one of lighter nuclei up to  $^{208}\text{Pb}$ . Already a small relative shift of one single-particle level can open up or close a gap in the spectrum.

- (iii) The strong Coulomb fields try to push the protons as far apart from each other as possible, and thereby to polarise the nucleus. Corrections to the Coulomb, isovector and surface energies that play no evident role for lighter nuclei might become crucial for SHE.

All of the above make predictions for the shell structure of superheavy nuclei in the island of stability a challenging task. The current situation can be summarised as follows:

- All widely used parametrisations of the single-particle potentials for macroscopic-microscopic models (Nilsson, Folded-Yukawa, Woods-Saxon) predict  $Z = 114$ ,  $N = 184$  as the dominant spherical shell closures in SHE [8, 15, 25, 27, 28, 29]. However, modifying the surface thickness of the single-particle potential might close the  $Z = 114$  gap and open up a gap at 126 instead [65, 66]. Note that the Woods-Saxon potential fitted by Chasman [15, 67] contains momentum-dependent terms that are not considered in the work of other groups.
- Self-consistent models using Skyrme, Gogny, or RMF interactions almost always give different doubly-magic nuclei than the standard macroscopic-microscopic models. They predict either  $Z = 120$  or 126 for the next proton shell closure and  $N = 172$  or 184 for the next neutron shell closure [32, 35, 37]. Not all combinations of these magic numbers are found, however. A notable exception is the SkI4 Skyrme parametrisation, which predicts  $Z = 114$  and  $N = 184$  like the macroscopic-microscopic models [35, 37].

Typical results that illustrate the lack of agreement between the models for proton single-particle states are displayed in Fig. 1. The comparison between  $^{298}_{184}114$  and  $^{292}_{172}120$  illustrates also that the single-particle spectra from self-consistent mean-field models change rapidly with proton and neutron numbers in this mass region [35, 37]. For example, the gap at  $Z = 120$  is much larger when the proton number takes this value than for the  $Z = 114$  isotope. A similar effect is found for the neutron shell closure at  $N = 172$  [37]. As can be seen in Fig. 1, predictions for the gaps in the single-particle spectra rarely exceed 2 MeV. In fact, it has been pointed out that the actual gaps themselves are no longer the decisive criterion for magicity in SHE [39]. This is illustrated in Fig. 2 that shows the shell correction determined from fully self-consistent mean-field calculations with the Skyrme interaction SLy6 for the tin region and for superheavy nuclei. For nuclei in the Sn region, the combined shell corrections for protons and neutrons are

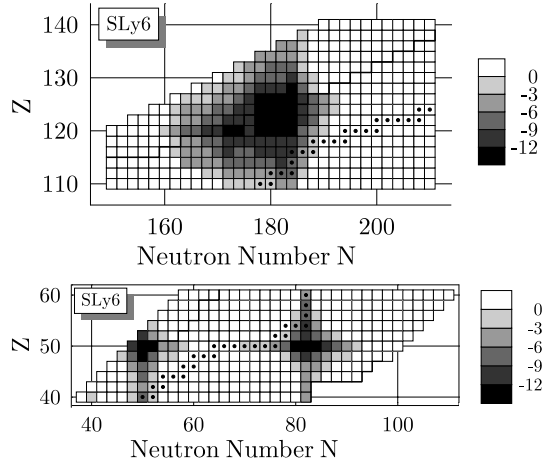


**Figure 2.** Total shell correction energy in MeV determined from fully self-consistent spherical calculations with the Skyrme SLy6 parametrisation for nuclei in the Sn region (bottom) and the transactinide region (top). Data taken from Ref. [39].

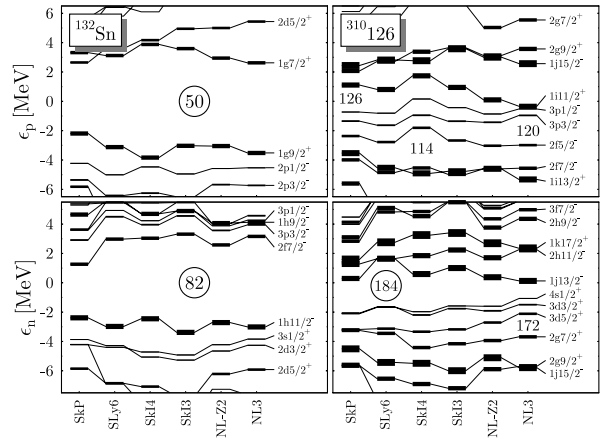


**Figure 3.** Proton (top) and neutron (bottom) single-particle levels of  $^{132}\text{Sn}$  (left) and  $^{310}_{184}\text{126}$  (right) obtained with the Skyrme (SkP-SkI3) and RMF (NL-Z2, NL3) interactions as indicated. To illustrate the degeneracy of the levels, their thickness is drawn proportional to  $2j + 1$ . Data taken from Ref. [39].

localised at the magic numbers  $Z = 50$ ,  $N = 50$  and  $N = 82$ . They take their largest values for the doubly-magic nuclei  $^{100}\text{Sn}$  and  $^{132}\text{Sn}$ , and fall off quickly when going away from them. The situation is very different for superheavy nuclei: here, the shell correction takes large values in a large region that ranges from  $N \approx 164$  to  $N \approx 184$  and  $Z \approx 114$  to  $Z \approx 126$ , and that encompasses all possible predictions for doubly-magic superheavy spherical nuclei. This finding is fairly independent of the chosen effective interaction [39]. It can be understood when recalling that the spherical single-particle levels have a  $(2j + 1)$ -fold degeneracy. The levels near the Fermi energy displayed in Fig. 1 range from  $j = 1/2$  up to  $15/2$ , and their degeneracy from 2 to 16. Its role can be better seen in the single-particle spectra displayed in Fig. 3, where the width of the levels is drawn proportional to their degeneracy. For spherical superheavy nuclei, the low- $j$  orbits of protons and neutrons are bunched amidst a large number of high- $j$  levels. Due to their large degeneracy, it are the latter that determine the average level density. The low- $j$  levels can be shifted around opening up or closing the gaps between them without making a large difference for the level density and the size of the shell correction, even when the corresponding single-particle spectra look very different. The low- $j$  are filled for proton numbers between 114 and 126 and neutron numbers between 172 and 184, which is exactly the zone where the combined shell correction is large. The appearance of bunched low- $j$  levels surrounded by high- $j$  levels follows trivially from the sequence of single-particle levels in a finite potential well and the spin-orbit splitting in nuclei that is large enough to push an intruder into the major shell below.

The appearance of the magic numbers  $Z = 120$  and  $N = 172$  in self-consistent models is the consequence of a polarisation of the density [37, 43, 44, 45, 52]. The low- $\ell$   $s$ ,  $p$ , and  $d$  orbits that were found to be crucial for the extra binding of spherical superheavy nuclei in the discussion above have as a common feature that their radial wave functions are localised well inside the nucleus. In general, only low- $\ell$  levels contribute to the density at small radii. Ignoring pairing and other correlations,  $^{292}_{172}\text{120}$  is the last nucleus for which they are not filled. By contrast, the occupied high- $\ell$  levels in the last major shell are all peaked on the the nuclear surface. Combining both, the net effect is a very pronounced central depression of both the proton and neutron densities, cf. Fig. 4, that has been characterised as a "semi-bubble" density



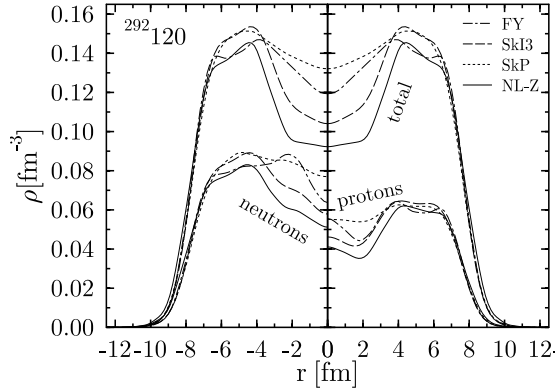


**Figure 4.** Radial profile of the neutron (left), proton (right) and total density of the spherical configuration of  $^{292}_{172}\text{120}$ , obtained with the Skyrme interactions SkI3 and SkP, the RMF Lagrangian NL-Z and the folded-Yukawa (FY) single-particle potential widely used in macroscopic-microscopic calculations. Data taken from Ref. [37].

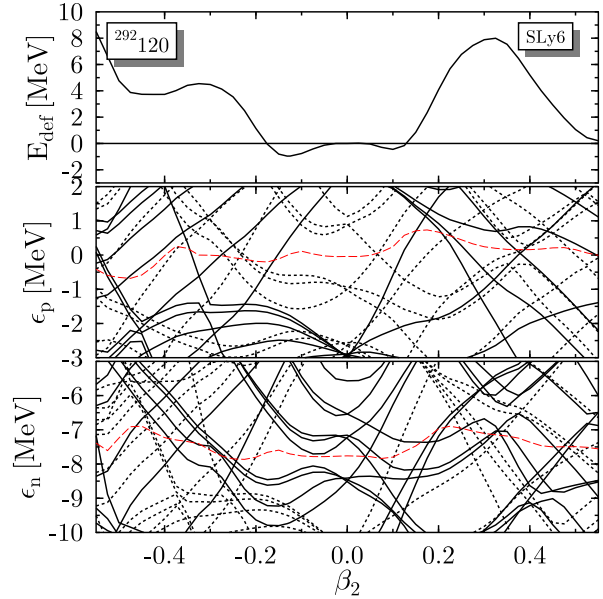


**Figure 5.** Axial deformation energy surface (top) and Nilsson diagrams of protons (middle) and neutrons (bottom) as a function of quadrupole deformation  $\beta_2$ , Eq. (2), as obtained with the Skyrme interaction SLy6 for  $^{292}_{172}\text{120}$ . In the Nilsson diagrams, solid (dotted) lines denote levels of positive (negative) parity. The Fermi energies of protons and neutrons are indicated with dashed red lines.

profile [44, 45]. In self-consistent models the density distribution feeds back onto the mean fields, in particular onto the radial profile of the spin-orbit potential [37]. For specific orbits such as the proton  $3p$  and neutron  $3d$  levels, the spin-orbit splitting is reduced to almost zero, cf. Fig. 1, which opens up the  $Z = 120$  and  $N = 172$  gaps. When filling the low- $j$  orbits one goes back to a regular density distribution and the gaps at  $Z = 120$  and  $N = 172$  disappear [37]. Similar, but weaker, effects can be seen in lighter nuclei. For those it is usually just the non-occupation of one proton or neutron low- $j$  level that causes a central depression of the density. The new feature of  $^{292}\text{120}$  is the much larger number of single-particle states and nucleons involved that makes the effect more pronounced. The size of this polarisation effect is correlated to the effective mass. It is the largest for small effective mass (NL-Z and SkI3 with  $m_0^*/m \approx 0.6$ ) and less pronounced for large effective mass (SkP,  $m_0^*/m = 1$ ). Interestingly, the density distribution from the folded-Yukawa (FY) single-particle potential frequently used in macroscopic-microscopic methods also exhibits a central depression, cf. Fig. 4. However, in the absence of self-consistency it neither feeds back onto the shell structure, nor onto the macroscopic energy.

Large gaps in the single-particle spectrum do not necessarily imply a spherical ground state. This is illustrated for  $^{292}_{172}\text{120}$  in Fig. 5. The deformation energy surface is quite soft around the spherical point ( $\beta_2 = 0$ ), with an oblate minimum at a  $\beta_2$  value of  $-0.13$ . Its softness is again related to the presence of low- $j$  levels around the Fermi energy for protons and neutrons. The splitting of their sub-states with deformation is rather weak and many of the levels on both sides of the Fermi surface repel each other such that the  $Z = 120$  and  $N = 172$  gaps persist far to the oblate side. The prediction whether  $^{292}\text{120}$  has a spherical or a deformed ground state, however, is very sensitive to details of the effective interaction. The Gogny force [44, 45, 48]

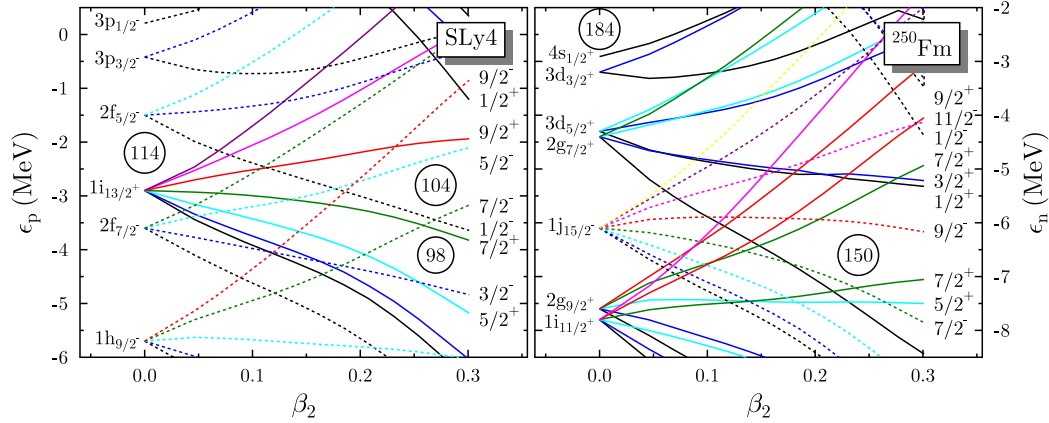


**Figure 6.** Nilsson diagrams of proton (left) and neutron (right) single-particle levels of  $^{250}_{150}\text{Fm}_{100}$  as obtained with the SLy4 Skyrme parametrisation [68] as a function of quadrupole deformation going from spherical shape to the prolate ground-state deformation. Labels on the left denote spherical  $j$  shells, labels on the right indicate  $j_z$  and parity. Levels of positive (negative) parity are drawn as solid (dotted) lines. The colours indicate different mean values of  $j_z$ .

and most Skyrme interactions [43, 69] give a similar result as SLy6, whereas a few other Skyrme interactions [43] and most relativistic mean-field models give a spherical minimum [69].

There is a large number of non-equivalent definitions of quadrupole deformations to be found in the literature, which is a source of confusion and misunderstandings when comparing results of different groups. Throughout this article we will use the dimensionless quadrupole deformation  $\beta_2$  that is obtained from the mean value of the quadrupole moment taking out its trivial scaling with proton and neutron number

$$\beta_2 \equiv \frac{4\pi}{3R^2A} \langle Q_{20} \rangle = \frac{4\pi}{3R^2A} \sqrt{\frac{5}{16\pi}} \langle 2z^2 - x^2 - y^2 \rangle, \quad (2)$$

where  $R = 1.2 A^{1/3}$  fm. Results from macroscopic-microscopic methods are usually shown in terms of the multipole expansion parameters of the nuclear surface, for which there exist several non-equivalent conventions and which are not equivalent to the mean values of the multipole moments [58]. Results from self-consistent models have also sometimes been presented in terms of shape expansion parameters estimated from the multipole moments [32, 34].

### 3. Deformed shell structure

We have seen above that there exists a multitude of conflicting predictions for the shell structure of spherical superheavy nuclei that constitute the "island of stability". As of today, the question about the location of the next shell closures cannot be answered by theory alone, and there is an ongoing effort to use the available spectroscopic data for well-deformed transactinides in the  $Z \approx 102$  region. The basic idea can be illustrated by the Nilsson diagram shown in Fig. 6, which covers deformations ranging from spherical shape to the prolate deformed ground state. At the ground-state deformation, the single-particle levels can be associated with the observed band heads of rotational bands in odd- $A$  nuclei. Measuring the energy differences between these band heads in the same nucleus and having a mean-field model that describes their relative positions, one can then estimate empirical spherical single-particle energies by tracing the Nilsson diagram back to spherical shape. The single-particle energies as they appear in the Nilsson diagram, however, are not observable. The differences between the energies of the various band heads measured differ from the single-particle energies in several respects. First, pairing correlations

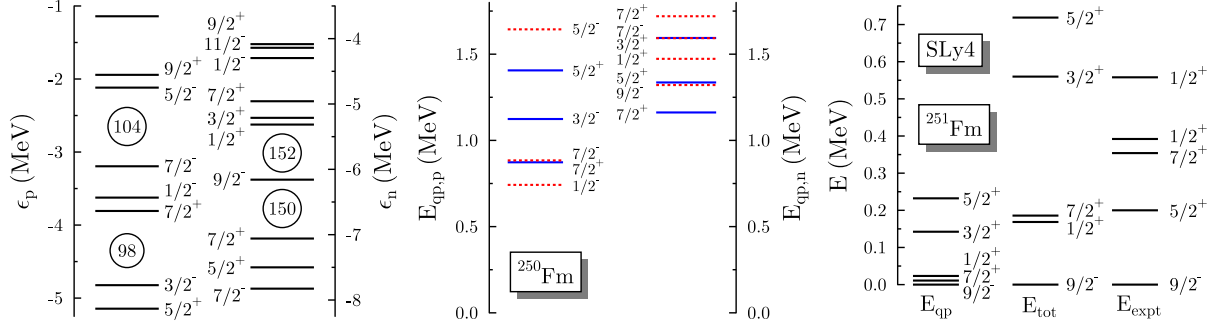


**Figure 7.** Spectrum of eigenvalues of the mean-field (left, Eq. (1)) and HFB Hamiltonian (middle, Eq. (3)) for protons and neutrons for the deformed ground state of  $^{250}\text{Fm}$  as obtained with the SLy4 Skyrme parametrisation. Solid blue (dashed red) lines indicate eigenvalues of the HFB Hamiltonian corresponding to single-particle levels below (above) the Fermi energy. The right panel compares the spectrum of eigenvalues  $E_{qp}$  of the HFB Hamiltonian for neutrons obtained for a HFB vacuum constrained to  $Z = 100$ ,  $N = 151$  and the spectrum of the energies from self-consistently calculated blocked HFB states  $E_{tot}$  in  $^{251}\text{Fm}$  with experimental data for band heads taken from [18]. All energies in the right panel are normalised to the ground state.

introduce a correction to the relative energies. Second, the unpaired nucleon polarises the mean fields. In particular, due to the lifting of Kramers degeneracy in an odd- $A$  nucleus, there is no useful way of representing single-particle energies as defined in Eq. (1) for the purpose of analysing the shell structure. Third, each configuration in an odd- $A$  nucleus has in general its own ground-state deformation. The effects of self-consistency when calculating these band heads are illustrated in Fig. 7. The left panel shows the single-particle spectra obtained for the ground state of  $^{250}\text{Fm}$ , which correspond to the end of the Nilsson diagrams in Fig. 6. Pairing correlations modify their relative energies. These are incorporated in the spectrum of eigenvalues  $E_{qp}$  of the HFB Hamiltonian

$$\begin{pmatrix} h & \Delta \\ -\Delta^* & -h^* \end{pmatrix} \begin{pmatrix} U \\ V \end{pmatrix} = E_{qp} \begin{pmatrix} U \\ V \end{pmatrix}, \quad (3)$$

often called quasi-particle energies and shown in the middle panel of Fig. 7. When neglecting off-diagonal matrix elements in the HFB equation (3), which leads to the simpler HF+BCS scheme, the quasi-particle energy of a single-particle level represents its distance from the Fermi energy  $\lambda$  and the size of its pairing gap  $\Delta_{\mu\bar{\mu}}$  through the relation  $E_{qp} \approx \sqrt{(\epsilon_{\mu} - \lambda)^2 + \Delta_{\mu\bar{\mu}}^2}$ . For a realistic pairing interaction, the values of the gaps  $\Delta_{\mu\bar{\mu}}$  strongly depend on the single-particle level. In full HFB, the coupling of the quasi-particle states through non-diagonal matrix elements slightly modifies the spectrum. The right panel of Fig. 7 compares two different calculations of the band heads in  $^{251}\text{Fm}$  with data. One is a perturbative calculation of these states from the spectrum of quasi-particle energies  $E_{qp}$  obtained from Eq. (3). The difference to the neutron spectrum in the middle panel of Fig. 7 is that the HFB vacuum is now calculated for particle numbers  $Z = 100$ ,  $N = 151$ . The readjustment of the Fermi energy for neutrons visibly rearranges the spectrum. In particular, the lowest quasi-particle state is now a  $9/2^-$ , in agreement with data. However, compared to experiment the spectrum of the  $E_{qp}$  is too compressed. Such perturbative calculation of low-lying states presents at best a crude approximation to the energies from full self-consistent calculations of the blocked HFB state for an odd- $A$  nucleus [70, 71], which is represented as  $E_{tot}$  in the right panel. In this case, the energy of each configuration results from a separate calculation of the quasi-particle excitation performed on an optimised vacuum. There are many rearrangement effects, such as a reduction of pairing when blocking a state,



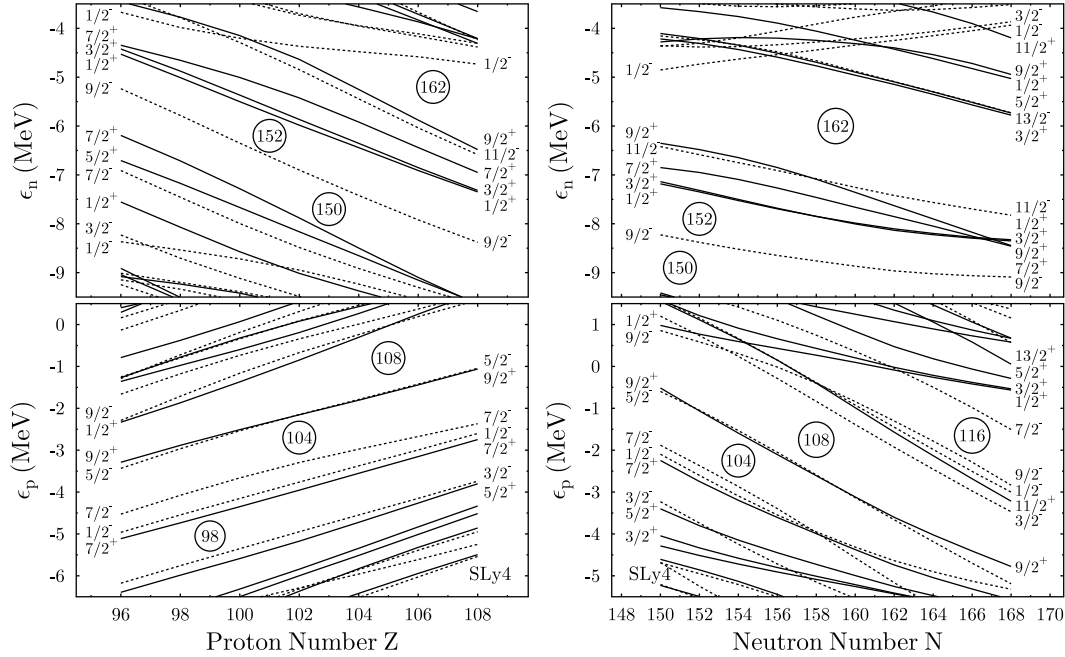


**Figure 8.** Single-particle spectra of neutrons (top panel) and protons (bottom) for the deformed ground states of  $N = 152$  isotones as a function of proton number (left) and of Hs ( $Z = 108$ ) isotopes as a function of neutron number (right) calculated with the SLy4 parametrisation of Skyrme’s interaction.

and changes in the mean fields and deformations, which are also all different for each blocked configuration. The net effect is that the spectrum of the  $E_{\text{tot}}$  is markedly different: the level sequence changes, and the spectrum is more spread out. The calculated level sequence, however, does not agree with data. In particular, the  $5/2^+$  level should be lower and the  $1/2^+$  level higher. This can be achieved by closing the  $N = 150$  gap in the single-particle spectrum and making the  $N = 152$  gap larger. The same modification of the single-particle spectrum is suggested by the analysis of adjacent odd- $A$  nuclei and by two-quasi-particle states observed as  $K$  isomers in even-even nuclei [18]. The presence of a deformed  $N = 150$  gap not seen in experiment in connection with a too small  $N = 152$  gap is a common problem of all self-consistent mean-field models using Skyrme [36, 42], Gogny [47] and relativistic mean-field interactions [36, 51, 53]. Similar problems are found for the single-particle spectra of protons, where a gap should be at  $Z = 100$ , not  $Z = 98$  and  $Z = 104$  [22, 36, 42, 47, 51, 53]. The deformed gaps are fairly reproduced by the single-particle potentials used in macroscopic-microscopic calculations, which explains their superiority for describing details of the spectroscopic data in the  $A \approx 250$  region.

In any event, the single-particle spectra, in particular in the form of Nilsson diagrams, are a more intuitive tool for the interpretation of shell structure than the spectra from self-consistent blocked states. We will use them in what follows to illustrate two further difficulties of establishing the link between deformed and spherical shell structures. The first of these difficulties is that the analysis cannot be done globally using the band heads of nuclei throughout the region of heavy nuclei. Instead, it has to be done locally, using only data from one or perhaps a few adjacent nuclei. The reason is that there are substantial changes in the single-particle spectra of the deformed ground states when varying  $N$  and  $Z$ , cf. Fig. 14. The nucleons rearrange themselves for the maximum gain in binding energy that is possible for a given number of particles. In particular, some of the deformed shell closures such as  $Z = 116$  and  $N = 162$  open up only for specific combinations of  $N$  and  $Z$ . The rearrangement of shells is accompanied

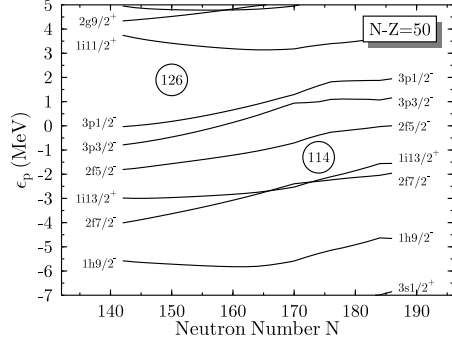


**Figure 9.** Evolution of *spherical* proton shell structure as predicted by the Skyrme SLy4 parametrisation when going from heavy actinides to superheavy nuclei along the  $\alpha$ -decay chain with  $N - Z = 50$ . For most nuclei shown, the spherical configuration corresponds to a local *maximum* of the energy surface, not a minimum. The spherical configuration of  $^{250}\text{Fm}$ , i.e.  $\beta_2 = 0$  in the left panel of Fig. 6, corresponds to  $N = 150$ .

by slight changes in all multipole moments and the density profile. The second difficulty is that also the spherical shell structure changes rapidly for heavy nuclei. This is illustrated by Fig. 9. Assuming for the moment that the effective interaction used would correctly describe the shell structure of nuclei around  $^{250}_{150}\text{Fm}_{100}$ , one would conjecture from the Nilsson diagram in Fig. 6 that there is a strong spherical  $Z=126$  shell closure. The  $Z=126$  gap, however, shrinks substantially when going to heavier nuclei, which is the effect already discussed in Fig. 1. In general, what is deduced about the magic numbers in the spherical single-particle spectrum in a non-magic nucleus might not be valid anymore for nuclei that actually have this magic number. Even when the SLy4 parametrisation does not describe all details of deformed shell structure in the  $Z \approx 100$  region, the rearrangement effects are generic to all self-consistent mean-field models.

The nucleon-number dependence of spherical shells as predicted by mean-field interactions is much stronger for SHE than for light elements, where the single-particle energies evolve much more slowly. In light nuclei, the observed strong quenching of various signatures of shell closures is only obtained when going beyond the self-consistent mean field [72, 73, 74, 75].

The deformed single-particle spectra are as sensitive to details of the effective interaction as are the spherical ones. Examples are given in Fig. 10 for Skyrme parametrisations with modified spin-orbit interactions. There are considerable changes relative to the Nilsson diagrams obtained

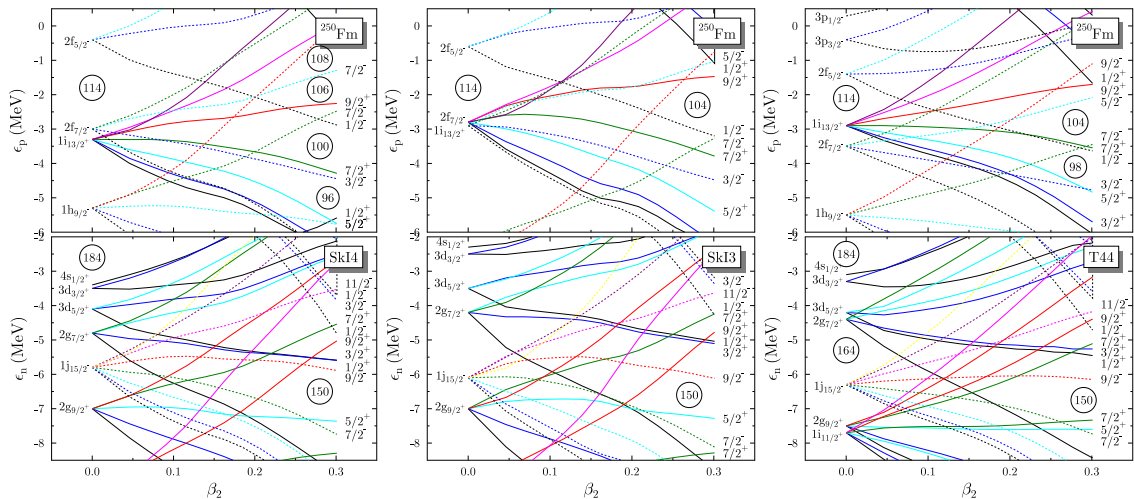


**Figure 10.** Parametrisation dependence of the Nilsson diagram of  $^{250}\text{Fm}$  for the example of three parametrisations of Skyrme's interaction. Left to right: SkI4 and SkI3 with two different non-standard choices of the isospin dependence of the spin-orbit field [76] and T44, which adds an explicit tensor force to a standard spin-orbit interaction [77].

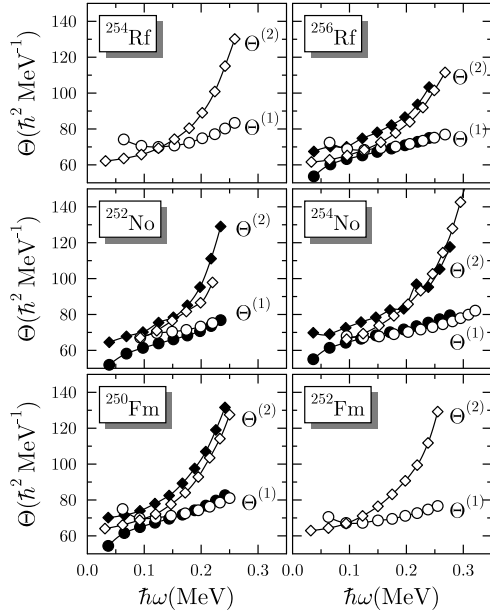


**Figure 11.** Kinematic ( $\Theta^{(1)}$ , circles) and dynamical ( $\Theta^{(2)}$ , diamonds) moments of inertia deduced from experiment (filled markers) and cranked HFB calculations with the SLy4 Skyrme parametrization (open markers). Calculated values taken from Ref. [42], experimental values from [18, 19] ( $^{250}\text{Fm}$ ,  $^{252,254}\text{No}$ ) and [79, 80] ( $^{256}\text{Rf}$ ).

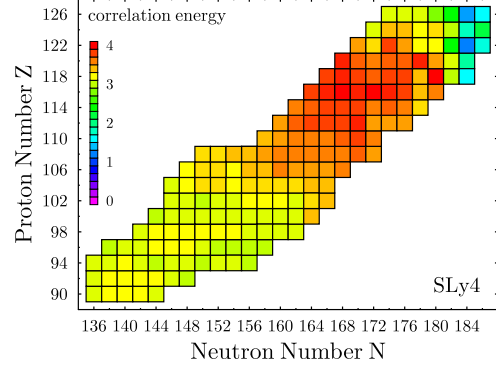


**Figure 12.** Quadrupole correlation energy in MeV from projection on angular momentum  $J = 0$  and mixing of axial configurations of different quadrupole deformation [78]. The correlation energy is defined as the difference between the energy of the particle-number projected mean-field ground state and the energy of the particle-number and angular-momentum projected GCM ground state, cf. [73]. Calculations were done with the SLy4 Skyrme parametrization.

with SLy4, cf. Fig. 6. However, for none of these parametrizations the deformed  $N = 152$  gap opens up. One improvement is found for SkI4, which gives a deformed  $Z = 100$  gaps like the macroscopic-microscopic models. This improves one- and two-quasi-particle spectra for proton excitations in the  $A \approx 250$  region [78]. However, it comes at the price of closing completely the  $N = 152$  gap, which deteriorates the spectra for neutron excitations [78].

The proof of large ground-state deformations in this region of the nuclear chart has been delivered by the observation of highly collective rotational bands, first for  $^{254}\text{No}$  [81], and then for some of its even-even and odd- $A$  neighbours [18, 19]. The observation of these bands triggered numerous cranked HFB calculations, where the mean-field equations are solved with an auxiliary condition on the mean value of angular momentum [40, 41, 42, 46, 51]. As an example, Fig. 11 compares calculations using the SLy4 Skyrme parametrization with data for some even-even nuclei. The figure displays the kinematical (first) moment of inertia  $\Theta^{(1)} \equiv J/\omega$  and the dynamical (second) moment of inertia  $\Theta^{(2)} \equiv dJ/d\omega = \Theta^{(1)} + \omega d\Theta^{(1)}/d\omega$  [18, 82] as a function of the rotational frequency  $\omega$ . The dynamical moment of inertia  $\Theta^{(2)}$  is a sensitive probe for the internal rearrangement of the nucleons with increasing angular momentum  $J$ . The calculations agree reasonably well with the data, although there are disagreements in detail, for example the slightly different up-bend of  $\Theta^{(2)}$  seen for  $^{252}\text{No}$  and  $^{254}\text{No}$ , which can be attributed to the deficiencies in the single-particle spectrum discussed above.

#### 4. Correlations beyond the mean field

The mean-field approximation is best justified for heavy nuclei whose ground state corresponds to a deep minimum in a stiff deformation energy surface. This is indeed the case for many

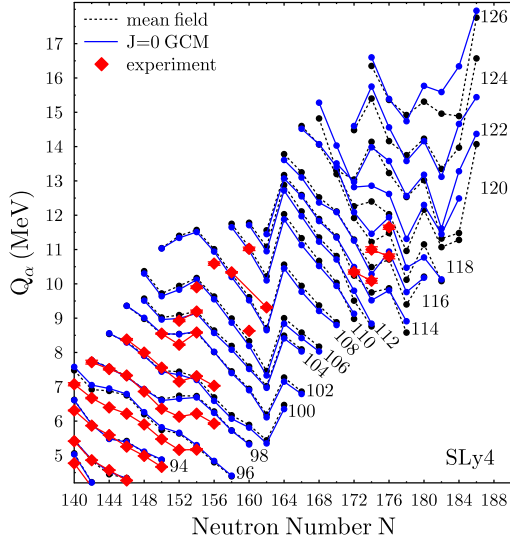


**Figure 13.**  $Q_\alpha$  values of even-even nuclei from self-consistent mean-field and beyond-mean-field calculations [78] with the Skyrme interaction SLy4 compared with data where available [85]. Lines connect values for isotopic chains as indicated by the labels.

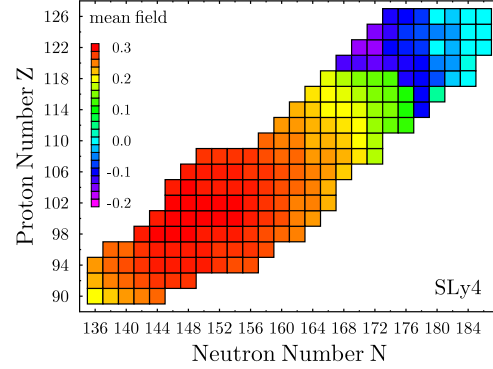


**Figure 14.** Dimensionless mass quadrupole moment  $\beta_2$  (2) of the ground state of heavy nuclei as obtained with the Skyrme interaction SLy4. Positive values denote prolate, negative values oblate deformations, whereas  $\beta_2 = 0$  indicates spherical shapes. Data taken from [78].

of the well-deformed mid-shell nuclei in the  $Z \approx 100$ ,  $N \approx 150$  region that are the object of detailed spectroscopic studies. By contrast, most of the heaviest recently synthesised nuclides and their daughter nuclei with  $Z \gtrsim 110$ ,  $N \gtrsim 164$  are in a region of transitional nuclei [34], which have soft deformation energy surfaces and in some cases also exhibit shape coexistence. For those, fluctuations in shape degrees of freedom or the mixing of coexisting shapes might have a significant impact on the ground state properties [72, 73, 74, 75, 56]. Both can be incorporated into the modelling in the framework of the generator coordinate method (GCM) [59, 60].

Figures 12 and 13 present results that consider pairing and quadrupole correlations beyond the mean field as described in Ref. [73]. The former are treated by projecting the mean-field state on good particle number. The nuclear shapes are restricted to axially symmetric and reflection-symmetric configurations. For these, the description of quadrupole correlations beyond the mean field simplifies from a five-dimensional calculation to the treatment of one Euler angle and the intrinsic deformation  $\beta_2$ . The same Skyrme interaction SLy4 is used together with a density-dependent pairing interaction to generate the mean-field states and for the configuration mixing. A detailed analysis of the ground-state correlations obtained in such calculations for nuclei up to  $Z \approx 100$  has been presented in Ref. [73]. These calculations were recently extended to superheavy nuclei [78]. The resulting beyond-mean-field ground-state quadrupole correlation energies are displayed in Fig. 12. Their behaviour is correlated to the ground-state deformation, Fig. 14, similar to what is found for the transition from the rare-earth to the lead region discussed in Ref. [73]. For the well-deformed nuclei below  $Z \lesssim 112$  and  $N \lesssim 166$  the correlation energy is dominated by rotational energy from angular-momentum projection. Its value is on the order of 3 MeV and almost constant, and much smaller than the static mean-field deformation energy that is on the order of about 20 MeV. The correlation energy takes larger values up to about 4 MeV for the transitional systems with  $116 \lesssim Z \lesssim 124$  and  $168 \lesssim N \lesssim 184$ , and then drops rapidly to small values of about 1.2 MeV for the rigid spherical nuclei close to the double shell closure  $Z = 126$ ,  $N = 184$ . For nuclei in the vicinity of spherical shell closures, the quadrupole

correlation energy is on the same order or even larger than the static deformation energy. The variation of the correlation energy offers an explanation for the characteristic pattern of the measured two-nucleon separation energies across shell closures [74] in nuclei up to the Pb region, which is not described by pure mean-field calculations. Figure 13 illustrates its impact on  $Q_\alpha$  values of very heavy nuclei. The difference between the mean-field and beyond-mean-field results is evidently largest where the correlation energy displayed in Fig. 12 varies quickly. This happens around the  $N = 184$  shell closure, where its variation from one nucleus to its daughter in an  $\alpha$ -decay chain might be as large as 3 MeV, and to a lesser extent for nuclei just below  $Z = 126$  and throughout the transitional region down to  $Z$  values around 110. By contrast, for the well-deformed nuclei with  $Z \approx 100$ , the  $Q_\alpha$  values are not significantly affected as the correlation energy is almost constant. When drawing the  $Q_\alpha$  values for isotopic chains as a function of neutron number as in Fig. 13, large gaps between the curves correspond to large deformed or spherical proton shell effects, whereas large downward jumps of the curves correspond to neutron shell effects. Both can be easily associated with the appearance of large gaps in the single-particle spectra displayed in Fig. 8. Again, the empirical shell effect at  $N = 152$  is not correctly described. This is a common deficiency of virtually all self-consistent mean-field models. On the mean-field level, very similar results are obtained also with other Skyrme interactions [36], the D1s parametrisation of the Gogny force [47, 48] and with relativistic mean-fields [36, 50]. It is noteworthy that the  $Q_\alpha$  values from macroscopic-microscopic methods also underestimate the discontinuity at  $N = 152$ , although they predict a sizable  $N = 152$  gap in the single-particle spectrum, cf. Ref. [30, 83]. Curiously, the beyond-mean-field correlation energy has a visible impact on energy differences only around spherical shell closures, but not deformed ones.

A similar method is the construction of a microscopic Bohr Hamiltonian through a series of approximations to projected GCM as described in Refs. [72, 75]. The study of selected  $\alpha$ -decay chains using a five-dimensional collective Bohr Hamiltonian in the full  $\beta_2$ - $\gamma$  plane derived from a relativistic mean-field has been recently presented in Ref. [56].

For some of the nuclei discussed here, considering only axial and reflection-symmetric shapes might not be sufficient. For some of the transitional nuclei in the  $Z \approx 116$ ,  $N \approx 170$  region, shallow triaxial minima have been predicted [34]. Nuclei with neutron number slightly larger than 184 might be reflection asymmetric in their mean-field ground states [48], which also hints at a possible octupole softness of adjacent nuclei. Likewise, based on the observation of low-lying  $2^-$  levels at energies below two times the pairing gap it has been argued that nuclei around  $N = 150$  might be soft in non-axial octupole degrees of freedom [84].

An alternative for the description of correlations beyond the self-consistent mean field is the framework of particle-vibration coupling (PVC). There, correlations are added as a diagrammatic expansion in terms of single-particle degrees of freedom and RPA phonons. This methodology is currently restricted to spherical nuclei. A study addressing singly- and doubly-magic  $Z = 120$  isotopes in the relativistic mean-field framework [54, 55] finds that the single-particle strength becomes highly fragmented, consequence of the small gap in the unperturbed single-particle spectrum. The single-particle levels are shifted toward the Fermi energy, such that the gap in the single-particle spectrum becomes smaller. With 4-5 MeV, the PVC correlation energies of even-even  $Z = 120$  nuclei reported in Ref. [55] are larger than the projected GCM values displayed in Fig. 12. However, these values should not be directly compared, as the former include also correlation energy from pairing which is not contained in the latter.

## 5. Conclusions

To summarise the main points of our discussion

- Because of the large density of single-particle levels, already small shifts of single-particle energies can qualitatively change the appearance of the single-particle spectra of SHE, which is not the case for lighter doubly-magic nuclei up to  $^{208}\text{Pb}$ .



- For SHE, the importance of the spherical shell closures for magicity is different than in lighter nuclei. Because of the presence of highly-degenerate high- $j$  levels and the smallness of the gaps in the single-particle spectrum, additional binding from quantal shell effects originates from the bunching of low- $j$  orbits near the Fermi energy, not from the gaps.
- It is not the magnitude of the shell effects that counts for the stabilisation of SHE, but how quickly it varies with deformation. One, sometimes even two, spherical shell closures do not automatically prevent superheavy nuclei from having a deformed mean-field ground state.
- Self-consistency induces many local structural changes in SHE.
- Their extrapolation to SHE amplifies differences between the models and parametrisations.
- Almost all models agree that neutron shell closures enforce sphericity much more than proton shell closures do. This finding, however, has to be taken with a grain of salt. As pointed out in Refs. [73, 74], mean-field models tend to overestimate the size of neutron shell gaps for shell closures throughout the chart of nuclei up to  $N = 126$ , whereas the proton shell closures are usually more satisfactorily described.
- Quadrupole correlations beyond the mean field affect mass differences such as  $Q_\alpha$  values in the transitional region between the well-deformed actinides and the spherical shell closures.

## Acknowledgments

This research was supported in parts by the French *Agence Nationale de la Recherche* under Grant No. ANR 2010 BLANC 0407 "NESQ", the CNRS/IN2P3 through the PICS No. 5994, the PAI-P6-23 of the Belgian Office for Scientific Policy and by the European Union's Seventh Framework Programme ENSAR under grant agreement n262010.

## References

- [1] Hofmann S 1998, *Rep. Prog. Phys.* **61**, 639
- [2] Armbruster P 1999 *Rep. Prog. Phys.* **62**, 465
- [3] Hofmann S and Münzenberg G 2000, *Rev. Mod. Phys.* **72**, 733
- [4] Armbruster P 2000, *Annu. Rev. Nucl. Part. Sci.* **50**, 411
- [5] Oganessian Yu Ts 2007 *J. Phys. G* **34**, R165
- [6] Hofmann S 2011 *Radiochim. Acta* **99**, 405
- [7] Heenen P-H and Nazarewicz W 2009 *Europhys. News* **33**, 1
- [8] Nilsson S G *et al.* 1968 *Nucl. Phys. A* **115**, 545 and 1969 *Nucl. Phys. A* **131**, 1
- [9] Meldner H 1969 *Phys. Rev.* **178**, 1815
- [10] Mosel U and Greiner W 1969 *Z. Phys.* **222**, 261
- [11] Köhler H S 1971 *Nucl. Phys. A* **162**, 385
- [12] Sobiczewski A, Krogulski T, Blocki J and Szymański Z, 1971 *Nucl. Phys. A* **168**, 519
- [13] Zagrebaev V, Karpov A and Greiner, W *contribution to this volume*
- [14] Eichler R *contribution to this volume*
- [15] Chasman R R, Ahmad I, Friedman A M and Erskine J R 1977 *Rev. Mod. Phys.* **49**, 833
- [16] Leino M and Heßberger F P 2004 *Annu. Rev. Nucl. Part. Sci.* **54**, 175
- [17] Herzberg R-D 2004 *J. Phys. G: Nucl. Part. Phys.* **30**, R123
- [18] Herzberg R-D and Greenlees P T 2008 *Prog. Part. Nucl. Phys.* **61**, 674
- [19] Herzberg R-D and Cox D M 2011 *Radiocim. Acta* **99**, 441
- [20] Herzberg R-D *et al.* 2006 *Nature* **442**, 896
- [21] Chatillon A *et al.* 2007 *Phys. Rev. Lett.* **98**, 132503
- [22] Chatillon A *et al.* 2006 *Eur. Phys. J. A* **30**, 397
- [23] Heßberger F P *et al.*, 2006 *Eur. Phys. J. A* **30**, 561
- [24] Block M *et al.* 2010 *Nature* **463**, 785
- [25] Ragnarsson I, Nilsson S G and Sheline R K 1978 *Phys. Rep.* **45**, 1
- [26] Nilsson S G and Ragnarsson I 1995 *Shapes and Shells in Nuclear Structure* (Cambridge University Press)
- [27] Möller P and Nix J R 1994 *J. Phys. G: Nucl. Part. Phys.* **20**, 1681
- [28] Sobiczewski A and Pomorski K 2007 *Prog. Part. Nucl. Phys.* **58**, 292
- [29] Sobiczewski A 2011 *Radiochim. Acta* **99**, 395

- [30] Baran A, Lojewski Z, Sieja K, Kowal M 2005 *Phys. Rev. C* **72**, 044310
- [31] Bender M, Heenen P-H, and Reinhard P-G 2003 *Rev. Mod. Phys.* **75**, 121
- [32] Ćwiok S, Dobaczewski J, Heenen P-H, Magierski P, Nazarewicz W 1996 *Nucl. Phys. A* **611**, 211
- [33] Ćwiok S, Nazarewicz W and Heenen P-H 1999 *Phys. Rev. Lett.* **83**, 1108
- [34] Ćwiok S, Heenen P-H, and Nazarewicz W 2005 *Nature* **433**, 709
- [35] Rutz K *et al.* 1997 *Phys. Rev. C* **56**, 238
- [36] Bürvenich T, Rutz K, Bender M, Reinhard P-G, Maruhn J A and Greiner W, 1998 *Eur. Phys. J. A* **3**, 139
- [37] Bender M, Rutz K, Reinhard P-G, Maruhn J A, Greiner W 1999 *Phys. Rev. C* **60**, 034304
- [38] Kruppa A T, Bender M, Nazarewicz W, Reinhard P-G, Vertse T, Ćwiok S 2000 *Phys. Rev. C* **61**, 034313
- [39] Bender M, Nazarewicz W, Reinhard P-G 2001 *Phys. Lett. B* **515**, 42
- [40] Duguet T, Bonche P, Heenen P-H 2001 *Nucl. Phys. A* **679**, 427
- [41] Laftchiev H, Samsen D, Quentin P, Piperova J 2001 *Eur. Phys. J. A* **12**, 155
- [42] Bender M, Bonche P, Duguet T, Heenen P-H 2003 *Nucl. Phys. A* **723**, 354
- [43] Pei J C, Xu F R and Stevenson P D 2005 *Phys. Rev. C* **71**, 034302
- [44] Dechargé J, Berger J-F, Dietrich K and Weiss M S 1999 *Phys. Lett. B* **451**, 275
- [45] Dechargé J, Berger J-F, Girod M and Dietrich K 2003 *Nucl. Phys. A* **716**, 55
- [46] Egido J L, Robledo J L 2000 *Phys. Rev. Lett.* **85**, 1198
- [47] Delaroche J-P, Girod M, Goutte H, and Libert J 2006 *Nucl. Phys. A* **771**, 103
- [48] Warda M and Egido J L 2012 *Phys. Rev. C* **86**, 014322
- [49] Lalazissis G A Sharma M M, Ring P and Gambhir Y K 1996 *Nucl. Phys. A* **608**, 202
- [50] Bender M 2000 *Phys. Rev. C* **61**, 031302(R)
- [51] Afanasjev A V, Khoo T L, Frauendorf S, Lalazissis G A, Ahmad I 2003 *Phys. Rev. C* **67**, 024309
- [52] Afanasjev A V and Frauendorf S 2005 *Phys. Rev. C* **71**, 064318
- [53] Afanasjev A V, Shawaqfeh S 2011 *Phys. Lett. B* **706**, 177
- [54] Litvinova E and Afanasjev A V 2011 *Phys. Rev. C* **84**, 014305
- [55] Litvinova E 2012 *Phys. Rev. C* **85**, 021303
- [56] Prassa V, Nikšić T, Lalazissis G A, and Vretenar D 2012 *Phys. Rev. C* **86**, 024317
- [57] Brack M and Quentin P, 1975 *Phys. Lett. B* **56**, 421; and 1981 *Nucl. Phys. A* 361, 36
- [58] Hasse R W and Myers W D *Geometrical relationships of macroscopic nuclear shapes*, 1988 (Berlin: Springer)
- [59] Egido J L and Robledo L M 2004 in *Extended Density Functionals in Nuclear Physics*, (Lecture Notes Phys. **641**) ed Lalazissis G A, Ring P and Vretenar D (Berlin: Springer) p 269.
- [60] Bender M 2008 *Eur. Phys. J. ST* **156**, 217
- [61] Simenel C, Wakhle, A and Avez, B *contribution to this volume*
- [62] Otsuka T *contribution to this volume*
- [63] Duguet T and Hagen G 2012 *Phys. Rev. C* **85**, 034330
- [64] Erler J, Birge N, Kortelainen M, Nazarewicz W, Olsen E, Perhac A M, Stoitsov M 2012 *Nature* **486**, 509
- [65] Anderson G, Larsson S E, Leander G, Nilsson S G, Ragnarsson I and Åberg S 1976 *Phys. Lett. B* **65**, 209
- [66] Patyk Z, Muntian I, Myers W D, Sobiczewski A and Swiatecki W J 1999 *Acta Phys. Pol. B* **30**, 693
- [67] Chasman R R 1971 *Phys. Rev. C* **3**, 1803
- [68] Chabanat E, Bonche P, Haensel P, Meyer J, Schaeffer R 1998 *Nucl. Phys. A* **635**; *ibid.* **643**, 441(E)
- [69] Bender M, Rutz K, Reinhard P-G, Maruhn J A, Greiner W 1998 *Phys. Rev. C* **58**, 2126
- [70] Duguet T, Bonche P, Heenen P-H and Meyer J 2002 *Phys. Rev. C* **65**, 014310
- [71] Bertsch G, Dobaczewski J, Nazarewicz W and Pei J 2009 *Phys. Rev. A* **79**, 043602
- [72] Fleischer P *et al.* 2004 *Eur. Phys. J. A* **22**, 363
- [73] Bender M, Bertsch G F, and Heenen P-H 2006 *Phys. Rev. C* **73**, 034322
- [74] Bender M, Bertsch G F, and Heenen P-H 2008 *Phys. Rev. C* **78**, 054312
- [75] Delaroche J-P *et al.* 2010 *Phys. Rev. C* **81**, 014303
- [76] Reinhard P-G and Flocard H 1995 *Nucl. Phys. A* **584**, 467
- [77] Lesinski T, Bender M, Bennaceur K, Duguet T, Meyer J 2007 *Phys. Rev. C* **76**, 014312
- [78] Bender M and Heenen P-H, *to be published*.
- [79] Greenlees P T *et al.* 2012 *Phys. Rev. Lett.* **109**, 012501
- [80] Rubert J *et al.* 2012 *contribution to this volume*
- [81] Reiter P *et al.* 1999 *Phys. Rev. Lett.* **82**, 509
- [82] Dudek J 1992 *Prog. Part. Nucl. Phys.* **28**, 132
- [83] Smolanczuk R 1997 *Phys. Rev. C* **56**, 812
- [84] Chen Y-S, Sun Y and Gao Z-C 2008 *Phys. Rev. C* **77**, 061305(R)
- [85] Super Heavy Elements Network, <http://www.transfermium.net>